Applications of active arrayed-waveguide grating in future wavelength division multiplexing networks

Article *in* Optical Engineering · March 2003

DOI: 10.1117/1.1541002

2 authors, including:

Fady I. El-Nahal
Islamic University of Gaza
32 PUBLICATIONS **57** CITATIONS

SEE PROFILE

Applications of active arrayed-waveguide grating in future wavelength division multiplexing networks

F. I. El-Nahal, MEMBER SPIE
R. J. Mears
Cambridge University
Engineering Department
Trumpington Street
Cambridge CB2 1PZ, United Kingdom
E-mail: fie20@eng.cam.ac.uk

Abstract. The role of active arrayed-waveguide gratings (AWGs) in future dynamic wavelength-division multiplexing (WDM) networking and routing is investigated. Simulations are done using the beam propagation method (BPM). The results indicate that active AWGs can be used in multiple-channel control with an SNR up to 19 dB and dynamic dispersion compensation of up to 160 ps/nm. [DOI: 10.1117/1.1541002]

Subject terms: beam propagation method; gratings; integrated optics; channel control; dispersion compensation; optical planar waveguide components; photonic switching systems; waveguide router; wavelength division multiplexing.

Paper 020202 received May 22, 2002; revised manuscript received Sep. 6, 2002; accepted for publication Sep. 6, 2002.

1 Introduction

The arrayed-waveguide grating (AWG), also known as a phased array (phasor), is emerging as a powerful tool in wavelength-division multiplexing (WDM) networks for passive multiplexing and fixed wavelength routing.[1–3]

Devices are generally made using lithographic methods in one of two main technologies: silica-based devices or InP-based devices. The low index contrast of silica limits the bend radii of the waveguides, so such devices are relatively large. InP-based devices[4] are far smaller, so there is a greater potential for integrating large number of devices.

Previous work[5–7] has demonstrated how an active AWG, an AWG with an array of phase modulators on its arrayed-waveguides section, provides some important aspects for dynamic WDM networking by means of holographic techniques based on the simulated annealing algorithm. An active AWG can be configured as an equalizing filter; a channel-dropping (suppressing) filter to yield optical add/drop multiplexing functionality; and a space/wavelength switch. Multiple channel control and dispersion compensation are attractive features of active AWG discussed here.

In this paper, we present for the first time, simulation results obtained using the beam propagation method (BPM), confirming the potential of using active AWG devices in multichannel control, and dispersion compensation. The results obtained here agree with earlier results obtained by means of Fourier methods.[7]

2 Beam Propagation Method (BPM)

Of all simulation techniques applied in the modelling of integrated and fiber optic photonic devices, BPM is the most widely used.[8] Figure 1 shows a schematic of an active AWG with both a phase hologram and an active symmetric parabolic phase profile imposed on its central arrayed-waveguide region (for illustration purposes, both the phase hologram and the parabolic phase profile are shown, but in a real configuration only one is used). Since AWG routers tend to be large structures, the resulting angle of propagation in an AWG varies to a large degree from the input to the output. As this requires the use of a wide-angle approximation (generally based on Padé approximations[9]), rather than a paraxial approximation, it would increase the computational load. To avoid this burdensome approach, the simulation process of the AWG was divided into three stages based on the assumption that the actual input, output, and the arrayed waveguides are decoupled a short distance away from the star couplers.

The first stage is a BPM simulation of the input star coupler at the center wavelength. This gives the relative amplitudes at the entrance of each arrayed waveguide. The second stage is a non-BPM simulation of the effect of arrayed waveguides, where the phase differences induced by each array arm are computed. The phase differences must be recalculated for every simulation wavelength that is used, i.e., the simulation of the array waveguides is wavelength dependent. In the final stage, the output star coupler is simulated with the inputs from each of the arrays. The wavelength used in the simulation of the input and output star couplers is not varied; only the wavelength in the waveguide grating is changed. This is a reasonable procedure, since the performance of the star couplers is largely wavelength independent over the narrow wavelength range of the AWG. The simplification enables the input star coupler to be simulated once, resulting in reduction of the computation time.

The ability to specify additional design information in the WDM router simulations using the BeamPROP package (from Rsoftinc) makes it easy to add arbitrary phase or length to each arrayed waveguide, also enabling modification of the transmission power in each arm. The phase holograms and the parabolic phase profile were imposed on the arrayed waveguides through this method.

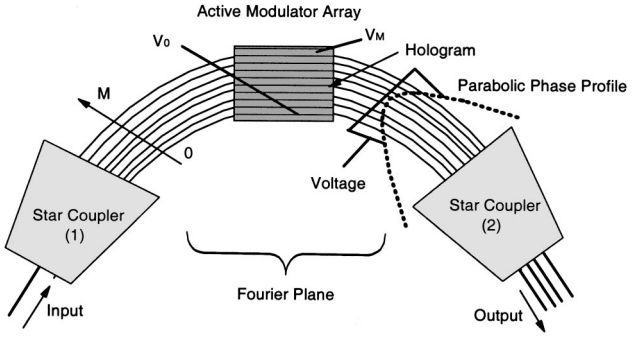

Fig. 1 Schematic of an active AWG with phase-modulators and parabolic phase profile in the Fourier plane.

3 Holographic AWG

An AWG can be considered as a planar 4-f lens relay system, where the two free propagating regions (FPRs) on either side of the arrayed-waveguide section can be modeled as lenses. This enables holographic techniques; based on Fourier transform (FT) theory, to be used as an effective tool to tailor the spectral response of AWGs, and achieve multichannel control, power equalization, and add/drop filtering.[7]

Using holographic techniques, the optical path length or phase of the arrayed-waveguides is varied to achieve the desired spectral response. Phase control of each arm can be achieved either by thermo-optic or electro-optic effects to actively alter the local refractive index of the individual waveguides. An arbitrary phase hologram Φ can be superimposed on the arrayed-waveguides section, which is the illumination plane, by means of an array of phase modulators,[10] as shown in Fig. 1. The far-field pattern is the FT of the aperture function, which is the product of the phase hologram transfer function, and an overall Gaussian amplitude distribution across the arrayed-waveguide section.

3.1 *Simulation Results*

Simulated annealing was used to calculate the holograms,[11] which were superimposed on the arrayed-waveguide section. The devices were then simulated using the BPM. An AWG model was built with the following parameters:

Center wavelength $(\lambda_0) = 1557.2$ nm
Number of input/output waveguides $= 8$
Number of arrayed waveguide $= 100$
Wavelength channel spacing $= 1.6$ nm
Grating order $= 122$
FPR effective index $(n_s) = 1.4532$
Waveguide effective index $(n_a) = 1.4513$
Background index $= 1.4482$
FPR length $(R_O) = 2754.53$ μm
Incremental path length difference $(\Delta L) = 130.904$ μm
Free spectral range (FSR) $= 12.8$ nm

The results obtained in this work used this model.

3.1.1 *Routing to specific port*

The ability to route the wavelength channel of interest to the desired AWG output port is of great importance. In a normal AWG, one wavelength channel appears at each output port. By using an optimized phase hologram, it is possible to choose that wavelength. Linear phase can do the job as well, however, phase holograms have the ability to control the signal passband width or power, and multiple-wavelength routing can be achieved, where more than one channel can appear at the same port.

The target [see Fig. 2(a)] is a square pulse in the position of the desired output channel; a more accurate mathematical model would convolve the implicit delta-function representation of each waveguide with the guided mode (an approximate Gaussian intensity distribution) structure of the light within the waveguide. However, the guided mode merely changes the overall envelope of the far-field intensity distribution, and can be neglected.[7] A plot of the optimization result is shown in Fig. 2(b), while the generated

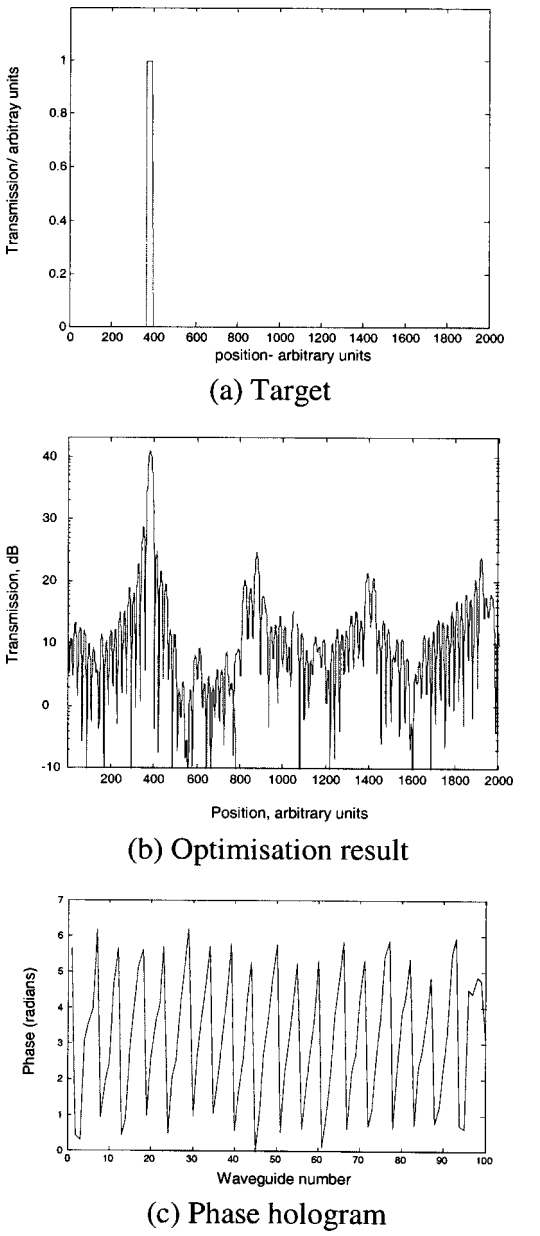

Fig. 2 (a) Target, (b) optimization result, and (c) phase hologram for a single channel.

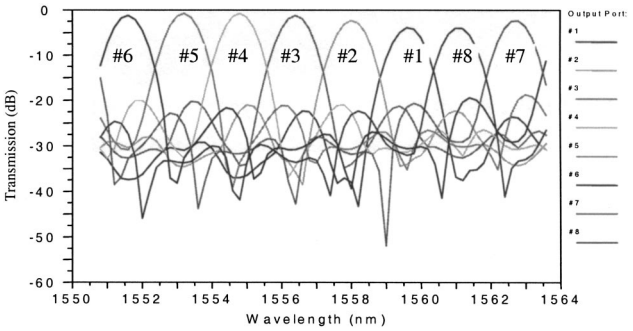

Fig. 3 Simulation of single channel hologram.

phase hologram for a single channel routing is shown in Fig. 2(c). These results were obtained using the simulated annealing algorithm.

The simulation result obtained for a single channel routing using BPM is shown in Fig. 3. The result shows that channel 6 has successfully been routed to the desired port (the output port where channel 1 would normally be) but the signal-to-noise ratio (SNR) has decreased significantly. In this case, the SNR is around 19 dB, which is close to the optimization result (20 dB) obtained using simulated annealing as shown in Fig. 2(b).

3.1.2 *Multiple-channel routing*

For multiple-channel routing, the devices were designed in the same way as the single-channel devices, except that the target function has multiple peaks, reflecting the number of routed channels. The selected channels are routed to the same output port. The BPM simulation results and the optimization results for multiple channel routing are shown in Fig. 4 for double-channels routing, and Fig. 5 for triple-channels routing.

The results show significant degradation of the SNR compared with the single-channel case, and the results vary for the different double-channel combinations. For example, channels 2/7 show lower uniformity but with an SNR of around 9 dB. For the triple-channel routing, channels 5, 6, and 7 were routed to port 8. The nonuniformity between the routed channels (around 3 dB) is clear from the BPM simulation results shown in Fig. 5. The SNR is

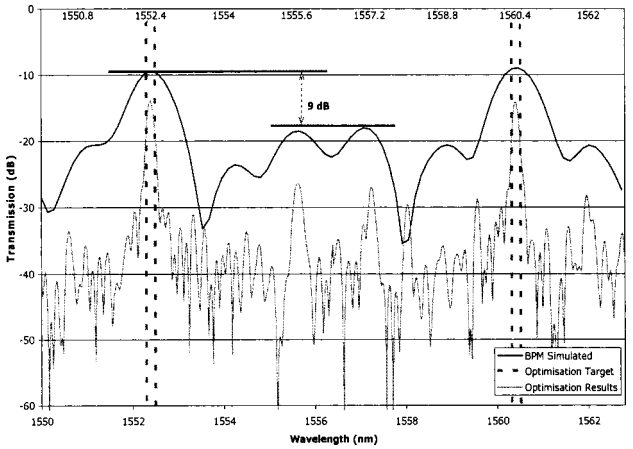

Fig. 4 Simulation of double-channel phase holograms.

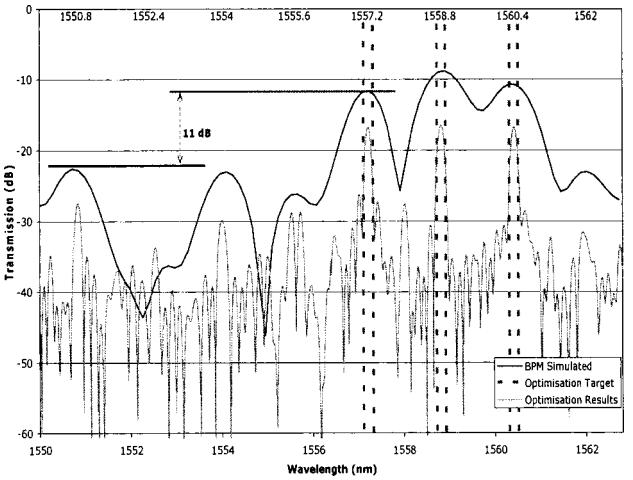

Fig. 5 Simulation of triple-channel phase holograms.

around 11 dB, which agrees with the optimization results. Further optimization of the phase hologram and higher number of arrayed waveguides will improve these figures.

3.1.3 *Phase errors*

The robustness of the holographic AWG design to fabrication tolerances is of great interest. The simulated annealing algorithm used to find the required hologram for a given output used quantized phase steps to reduce execution time. Previous work using FT models[7] found $\pi/8$ as a reasonable phase step, giving minimal excess distortion on the output amplitudes. These findings were tested using the BPM. Random phase errors ($\phi_e = \pi/8$, $\pi/4$, $\pi/2$, and π) corresponding to pathlength jitter of $\lambda/16$, $\lambda/8$, $\lambda/4$, and $\lambda/2$ were simulated. The result for $\lambda/4$ is shown in Fig. 6. The results show a change in the SNR for the different phase errors. The effect of the phase error $\pi/8$ is barely noticeable. For phase error of $\pi/4$, the SNR is around 17 dB. The design starts to break down for path-length jitter of $\lambda/4$, where the SNR is less than 7 dB. These results justify the use of a phase step of $\pi/8$ and indicate that the holographic designs are robust to individual phase modulator failures and fabrication phase errors.

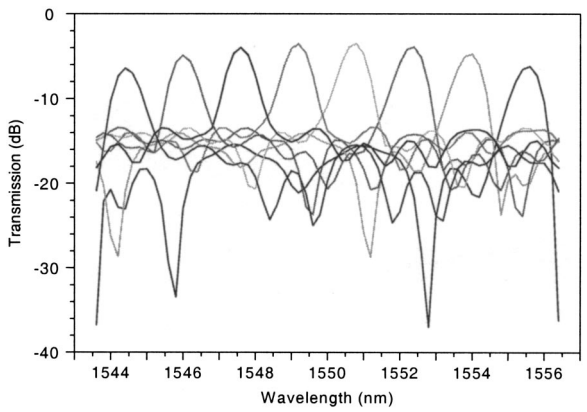

Fig. 6 Effect of random phase error of $\pi/2 = \lambda/4$ (path-length jitter).

3.1.4 *Holographic AWG excess insertion loss*

Applying a phase hologram on the arrayed-waveguides section results in extra insertion loss, as the grating becomes less efficient at routing light to the output port. According to Ref. 12, the excess insertion loss increases with the number of channels being controlled. The results obtained here show that the insertion loss is approximately 1 dB for single-channel routing, around 5 to 6 dB for double-channel routing, and 7 to 9 dB for triple-channel routing.

4 Dynamic Dispersion Compensation

Dispersion compensation techniques are a critical element in designing high-capacity lightwave communication systems. Static dispersion compensation can be done using dispersion compensation fiber[13] (fiber with the opposite dispersion, so that the total dispersion can be reduced) or fiber Bragg gratings.[14] Dynamic compensation is extremely important as many different signals take entirely different paths through optical networks.

4.1 *Parabolic Arrayed-Waveguide Gratings (P-AWGs)*

Here we consider the approach of using an AWG with a parabolic phase profile applied on the arrayed-waveguide section, as shown in Fig. 1. The parabolic phase profile has the potential to control[7] the dispersion of an AWG. The dispersion can be varied by adjusting the amount of parabolic phase shift induced.

The dispersion $D(\lambda)$ given in Eq. (1) is defined as the wavelength derivative of the group delay $G(\lambda)$. Group delay is defined as the negative angular frequency derivative of the phase response:

$$D(\lambda)=\frac{\partial G(\lambda)}{\partial \lambda}\approx\frac{\lambda_0^2}{2\pi c}\frac{\partial^2\phi(\lambda)}{\partial\lambda^2}. \tag{1}$$

According to Ref. 7,

$$D\approx\frac{M^4\lambda_0^3\pi^2}{45c\mathrm{FSR}^3}\left(1-\frac{12\alpha^2}{315}\right)B, \tag{2}$$

where D is the dispersion in sm^{-1}; λ_0 is the wavelength of the signal; c is the speed of light in vacuum; ϕ is the phase of the signal; M is the total number of arrayed waveguides; FSR is the free spectral range; B is the voltage-dependent coefficient, which controls the strength of the induced parabolic phase shift, equivalent also to the degree of chirp imposed on the device; and α is the Gaussian parameter to vary the power profile across the arrayed waveguides. Equation (2) is explained in detail in Ref. 7.

The power in waveguide m in the array is equal to constant$\times\exp[-\alpha_n(m-M/2)^2]$, where $\alpha_n=\alpha(2/M)^2$ is the normalized Gaussian apodization parameter. For a dispersive AWG, the phase in waveguide m is equal to

$$\frac{2\pi n\Delta l}{\lambda}\left[m+B\left(m-\frac{M}{2}\right)^2\right],$$

$$B=\frac{\mathrm{FSR}}{2\pi M^2\lambda_0}F,$$

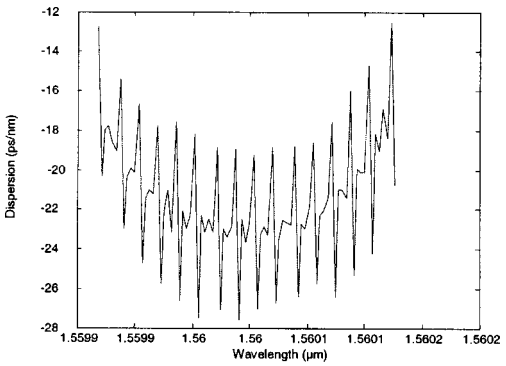

(a) Dispersion characteristics, F = 0

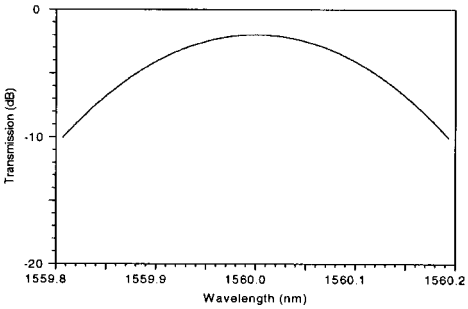

(b) Transmission characteristics, F = 17.6

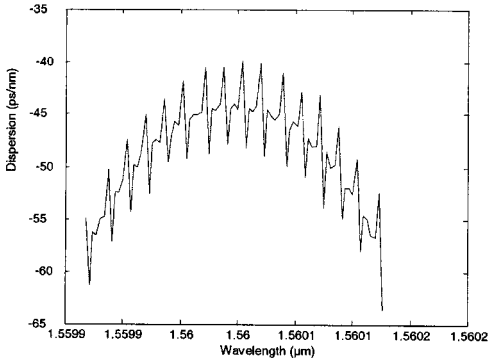

(c) Dispersion characteristics, F = 17.6

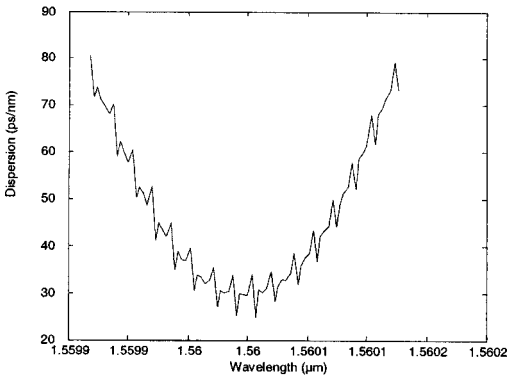

(d) Dispersion characteristics, F = -17.6

Fig. 7 Transmission and dispersion characteristics for $M=128$ P-AWG: (a) dispersion characteristics, $F=0$; (b) transmission characteristics, $F=17.6$; (c) dispersion characteristics, $F=17.6$; and (d) dispersion characteristics, $F=-17.6$

Table 1 The 3-dB passband width and the dispersion characteristics of $M=64$, 128 P-AWG filters.

	$M=64$			$M=128$		
	Approximated 3-dB Passband (nm)	Approximated 30-dB Bandwidth (nm)	Approximated Dispersion (ps/nm)	Approximated 3-dB Passband (nm)	Approximated 30-dB Bandwidth (nm)	Approximated Dispersion (ps/nm)
Unchirped AWG	0.3805	1.1	−3	0.1939	0.534	−22
$F=17.6$	0.4537	1.5	−10.7	0.2341	0.9	−45
$F=-17.6$	0.4024	1.455	10.5	0.1866	0.72	30

where Δl is the incremental path length difference, n is the refractive index of the arrayed waveguides, λ_0 is the central wavelength, and F is the normalized chirp parameter and is proportional to B.

Thus the phase in waveguide m is given by two components:

1. One is $(2\pi n\Delta lm)/\lambda$, which is the linear phase for a standard AWG.
2. The other is $(2\pi n\Delta l/\lambda)(m-M/2)^2B$, which is the additional phase applied to the waveguide arm to achieve the desired spectral response for the AWG design. In this case, this is equivalent to chirping the AWG to make it dispersive.

The simulation results in this paper were obtained using the BPM to compute the optical fields.

As mentioned before, the dispersion characteristic is defined as the second-frequency derivative of the AWG phase response, but can be closely approximated by Eq. (1). Dispersion can thus be calculated by measuring the phase of the output signal across the passband for a particular AWG output port. Using BeamPROP, the wavelength was swept across the passband of the central channel, and the power/phase were calculated for each wavelength; 120 wavelength points were used. These phase values were then used to compute the dispersion using Eq. (1).

4.2 *Simulation Results*

Several active AWGs were modeled, and the variation of dispersion with different design parameters such as M, α, and F was tested.

4.2.1 *Total number of arrayed waveguides (M)*

As M is increased, the dispersion should also increase, since the overall ''length'' of the AWG given approximately by $M\Delta l$ is increasing. If the device length is increasing, then there is a greater time delay through the device between fastest and slowest pulses along the shortest and longest waveguides respectively. Hence it is more dispersive.

Two different arrayed-waveguides numbers, $M=64$, FSR$=(15\times0.8\text{ nm})=12$ nm, and $M=128$, FSR$=(31\times0.39\text{ nm})=12$ nm, of parabolic AWGs, arrayed-waveguide refractive index $n_g=2.2$, central wavelength $\lambda_0=1560$ nm were simulated using the BPM for different chirp parameters, $F=0$ (unchirped AWG), $F=\pm17.6$. (Note that $F=\pm17.6$ was used because earlier Fourier analysis[7] suggested this value for maximum dispersion.)

Figure 7 shows the transmission and dispersion characteristics for $M=128$ P-AWGs. Comparison between the two filters is included in Table 1.

4.2.2 *FSR*

The FSR is given by FSR$=N\ \Delta\lambda_s$, where N is the number of channels, and $\Delta\lambda_s$ is the wavelength spacing between adjacent channels. A comparison between two ($M=128$) P-AWGs with different $\Delta\lambda_s$ is shown in Table 2. The results in Table 2 show that the dispersion increases with reducing $\Delta\lambda_s$.

4.2.3 *Chirp factor F*

According to Ref. 7, the dispersion increases linearly with the chirp factor F or the voltage-dependent coefficient B, until a maximum is reached for $F=\pm17.6$. Then the dispersion rapidly decreases. Here, the same AWG with $M=128$ was modeled for different chirping factors F. The variation of the dispersion as a function of F is plotted in Fig. 8. It is apparent from the plot that there is an initial increase in dispersion with chirp F, until a maximum is reached. However, the dispersion characteristics are not

Table 2 Dispersion variation with $\Delta\lambda_s$.

F	Dispersion (ps/nm), $\Delta\lambda_s=0.39$ nm	Dispersion (ps/nm), $\Delta\lambda_s=0.8$ nm
0	−22	−5.3
17.6	−45	−10.3
−17.6	30	7

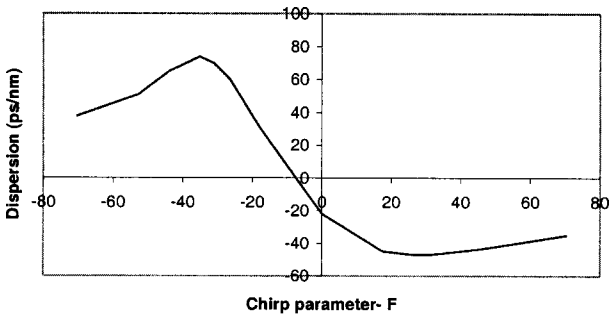

Fig. 8 Variation of dispersion with chirp parameter F.

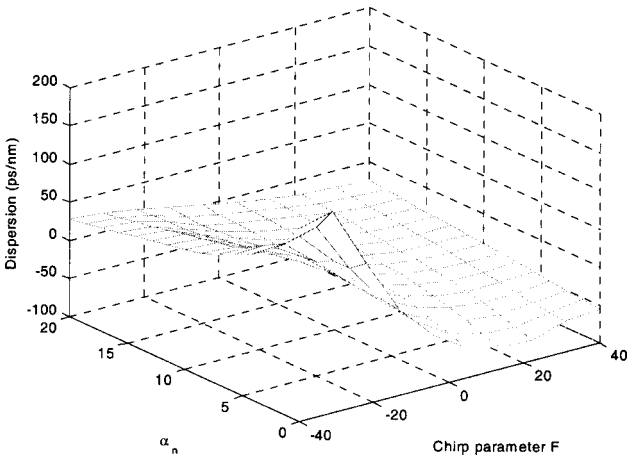

Fig. 9 Mesh plot of variation of dispersion with chirp parameter F and normalized apodization parameter α_n.

symmetric around $F=0$. The maximum positive dispersion is reached for $F\approx -35$, before declining. Maximum negative dispersion is reached around $F=17.6$ but the dispersion remains nearly constant for any further increase in F.

The 3-dB passband linearly increases with the chirp parameter F, the expression relating F to $\Delta\lambda_{3\mathrm{dB}}$ according to Ref. 7 is

$$\Delta\lambda_{3\mathrm{dB}}\approx\Delta\lambda_0\left(1+\frac{F}{4}\right).$$

The results showed the increase of 3-dB passband by increasing F. The 3-dB passband was 0.2341 nm for $F=17.6$, climbing to 0.2707 nm for $F=26.4$.

4.2.4 *Gaussian parameter α*

According to Ref. 7, the dispersion is maximized when the Gaussian parameter $\alpha=0$, i.e., applying a uniform power distribution along the arrayed waveguides. Using the same AWG model ($M=128$) as in the last section, several AWG models were simulated for different values of α and F. Figure 9 shows a 3-D mesh plot of the variation of dispersion D as it varies with chirp parameter F and normalized Gaussian apodization parameter α_n. From the plot it is clear that dispersion is maximized for a uniform power distribution along the arrayed waveguides, and it is reduced by increasing α. Dispersion in the range of -80 to 165 ps/nm was obtained.

4.2.5 *Dispersion variation across the output ports*

So far the dispersion characteristics were calculated only across the 3-dB passband of the central channel. The variation of dispersion across the other output ports/channels is of great interest. Figure 10 shows the variation of dispersion across different output ports for the $M=128$ P-AWG described before. It is clear from the plot that the dispersion is almost constant through the AWG output ports.

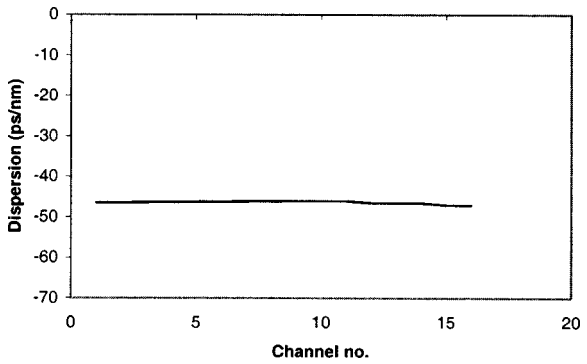

Fig. 10 Dispersion across the output ports of the filter.

4.2.6 *Excess insertion loss due to chirping of waveguide grating*

Figure 11 shows the transmission as a function of the chirp parameter F. The graph indicates the general trend in reduction of device transmission with varying chirp. This can be explained by the fact that the chirp process is analogous to the effect of a defocusing lens causing a reduction in intensity of light at the focal plane, and therefore introduces extra loss.

Assuming an AWG with zero chirp, Fig. 11 indicates transmission of -1.03 dB. The transmission for a device with chirp parameter $F=17.6$ is -1.99 dB. Hence the excess insertion loss due to the chirp effect for this particular device is around 0.96 dB. For a device with chirp parameter $F=31$ according to Fig. 11, the excess insertion loss is approximately 1.91 dB. The results obtained here show less excess insertion loss due to chirping compared with the results obtained in Ref. 7.

4.3 *Discussion*

The results do agree with the trend in the theoretical values computed using Fourier methods.[7] However, there are some differences that need to be addressed. First, the points of agreement are

1. As M is doubled from 64 to 128, the dispersion increases by a factor of 4, and the 3-dB passband width is approximately halved.
2. The results indicate that there is a positive and negative dispersion when F is negative or positive, respectively. The dispersion increases with F until a

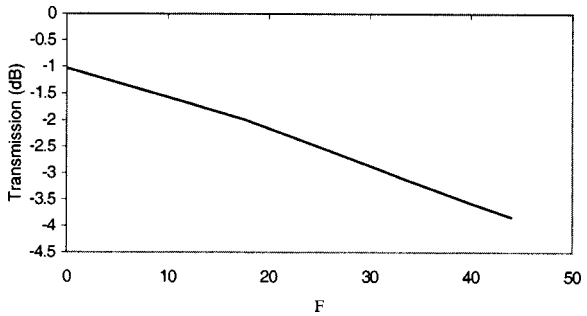

Fig. 11 Variation of transmission as a function of chirp parameter F.

maximum is reached before dropping again; however, the maximum here is not at $F=\pm 17.6$. The 3-dB passband also increases with F.

3. We can see from the results, that first, the dispersion has increased markedly by applying a uniform power distribution across the arrayed waveguides; second, they are much closer to the theoretically expected values computed using Fourier model; and third, the dispersion is reduced by increasing α, which agrees with Fourier model.

The results contain some aspects that differ from those which would be expected. The first thing we recognize is that the dispersion for the linear unchirped filter ($F=0$) is not zero. The ideal AWG filter should have perfectly linear phase and therefore constant time delay and no dispersion. However, it has shifted to -3 ps/nm for $M=64$ P-AWG and -22 ps/nm for $M=128$ P-AWG. This can be explained as a result of inherent waveguide dispersion.

1. The plot of variation of dispersion with chirp parameter F in Fig. 8 shows some kind of symmetry around a negative value of F between 0 and -20 instead of $F=0$.
2. The dispersions are lower than theoretically predicted, especially for AWGs with normal power distributions across the arrayed waveguides (no change has been made to the power profile across the arrayed waveguides). Possible explanations include the fact that the parameter α is rather large. (Most of the power is concentrated in the central arrayed waveguides.)
3. The 3-dB passband widths for the unchirped AWGs are much larger than theoretically predicted, in contrast to the chirped AWGs, which are smaller than theoretically predicted. A possible explanation for this is the large value of α.
4. The dispersion profiles across the 3-dB passband widths exhibit a strong ripple, and also have an overall parabolic-looking underlying tendency. The dispersion profile is expected to be much smoother, and to have a more pronounced straight-line underlying tendency. One explanation for this is that the 120 wavelength points are not sufficient to calculate the appropriate second-order differential phase response. Again, this could also be due to the large value of α.

4.4 *Dispersion Compensation Optimization*

To improve the dispersion compensation characteristics of P-AWG, some design parameters need to be optimized. The dispersion of the parabolic AWG is mainly dependent on the number of arrayed waveguides (M), FSR, apodisation parameter α, and the chirp parameter F. The dispersion can be improved by increasing M, i.e., by increasing the physical size of the device. A large P-AWG has a larger dispersion.

The FSR is another important factor that can optimize the dispersion. Decreasing $\Delta\lambda_{\text{spacing}}$, as suggested by Ref. 7, results in an increase in dispersion. Applying a uniform power distribution along the arrayed waveguides increases dispersion. This can be achieved if the input star coupler section consists of a multimode interference coupler.[4]

5 Conclusions

In conclusion, we have described how ''active AWGs'' have a variety of potential applications in future WDM networks. While earlier work[7] has modeled active AWGs using simple Fourier methods, the simulations presented in this paper were performed using the BPM, which is expected to be more accurate. In the first section of the paper a ''phase-only'' holographic technique to achieve channel control was described. Single-channel routing was simulated, with interchannel amplified spontaneous emission (ASE) suppressed by around 19 dB. Multichannel routing was achieved but with higher SNR around 10 dB. These figures can be improved by further optimizing the phase hologram and by increasing the number of arrayed waveguides. The holographic designs were robust to fabrication phase errors, and phase-modulator failures.

Dispersion compensation is another attractive potential feature of the active AWG described here. Dispersion compensation from -80 to 160 ps/nm was achieved using a P-AWG. Higher dispersion compensation rates can be achieved by tailoring some design parameters of the AWG. The variable dispersion feature may also be useful in all-optical IP routers, where packet time alignment and jitter reduction are important issues.

Acknowledgments

This work is supported by the Engineering and Physical Sciences Research Council (EPSRC). We would like to thank Michael C. Parker for his help.

References

1. M. K. Smit, ''New focusing and dispersive planar component based on an optical phased array,'' *Electron. Lett.* **7**(24), 385–386 (1988).
2. G. R. Hill, ''A wavelength routing approach to optical communication networks,'' *Brit. Telecom. Technol. J.* **3**(6), 24–31 (1988).
3. M. C. Parker, F. Farjady, and S. D. Walker, ''Wavelength-tolerant optical access architectures featuring *N*-dimensional addressing and cascade arrayed waveguide gratings,'' *J. Lightwave Technol.* **12**(16), 2296–2302 (1998).
4. M. Zirngibl, C. Dragone, and C. H. Joyner, ''Demonstration of a 15 $\times$15 arrayed waveguide multiplexer on InP,'' *IEEE Photonics Technol. Lett.* **11**(4), 1250–1253 (1992).
5. G. A. Lampropoulos, A. U. G. Signals Ltd., ''Application of synthetic aperture techniques to arrayed-waveguide grating passband control,'' in *Proc. IPR'98*, Victoria, B.C., Canada, (1998).
6. M. C. Parker and S. D. Walker, ''Design of arrayed-waveguide gratings using hybrid Fourier-Fresnel transform techniques,'' *IEEE J. Selec. Top. Quantum Electron. Fibre-Optic Passive Comp.* **5**(5), 1379–1384 (1999).
7. M. C. Parker, S. D. Walker, A. Yiptong, and R. J. Mears, ''Application of active arrayed-waveguide gratings in dynamic WDM networking and routing,'' *J. Lightwave Technol.* **12**(18), 1749–1756 (2000).
8. D. Yevick, ''A guide to electric field propagation techniques for guided-wave optics,'' *Opt. Quantum Electron.* **3**(26), 185–197 (1994).
9. G. R. Hadley, ''Wide-angle beam propagation using Pade approximant operators,'' *Opt. Lett.* **20**(17), 1426–1428 (1992).

10. D. H. P. Maat, F. H. Groen, R. C. Horsten, Y. C. Zhu, P. E. W. Kruis, C. G. P. Herben, X. J. M. Leijtens, and M. K. Smith, ''Tunable phase array demultiplexer on InP featuring wide-range tuning and passband shaping,'' in *Proc. ECIO'99*, Turin, Italy (1999).
11. T. D. Wilkinson, D. C. O'Brien, and R. J. Mears, ''Dynamic asymmetric binary holograms using a ferroelectric liquid crystal spatial light modulator,'' *Opt. Commun.* **3–4**(109), 222–226 (1994).
12. A. D. Cohen, M. C. Parker, and R. J. Mears, ''100-GHz-resolution dynamic holographic channel management for WDM,'' *IEEE Photonics Technol. Lett.* **7**(11), 851–853 (1999).
13. C. K. Madsen and J. K. Zhao, *Optical Filter Design and Analysis*, John Wiley & Sons, New York, (1999).
14. F. Ouellette, J.-F. Cliché, and S. Gagnon, ''All-fibre devices for chromatic dispersion compensation based on chirped distributed resonant coupling,'' *J. Lightwave Technol.* **10**(12), 1727–1738 (1994).

F. I. El-Nahal received his BSc degree in electrical and electronic engineering in 1996 from Alfateh University and his MPhil degree in microelectronic engineering in 2000 from Cambridge University, where he is currently a PhD student in the Engineering Department. His research activities include optoelectronics, optical communications and wavelength routing in optical networks.

R. J. Mears: Biography and photograph not available.